Supporting Information

Reversible Chemical Delithiation/Lithiation of LiFePO$_4$: Towards A Redox Flow Lithium-ion Battery

Qizhao Huang[a], Hong Li[b], Michael Grätzel[c], Qing Wang[a],*

[5]

[a]*Department of Materials Science and Engineering, Faculty of Engineering, NUSNNI-NanoCore, National University of Singapore. Block E2, #05-27, 5 Engineering Drive 2, 117576Singapore. Fax: (65) 6776-3604; Tel: (65) 6516-7118; E-mail: msewq@nus.edu.sg*
[b]*Key Laboratory for Renewable Energy, Institute of Physics, Chinese Academy of Sciences, Beijing,*
[10] *100080, China*
[c]*Laboratory of Photonics and Interfaces, Faculty of Basic Science, École Polytechnique Fédérale de Lausanne,CH-1015, Lausanne, Switzerland.*

1. Methods

[15] **Electrochemical Tests**

All the electrochemical tests were performed with a Multi-Channel Electrochemical Analyser (Ivium). Unless otherwise stated, all electrolyte used was 1 M LiPF$_6$/DMC:EC (1:1 vol%). 5 mM ferrocene (Fc, Acros, 98 %) and 1,1-dibromoferrocene (FcBr$_2$, Sigma Aldrich, 97%) solutions were used for the cyclic voltammetry (CV). Commercial LiFePO$_4$ (Sigma Aldrich) was used as received.
[20] The working electrode was a platinum disc, and both the reference and counter electrodes were Li foils. For the galvanostatic charge/discharge measurements, 20 mM redox molecules were dissolved in 1 ml of electrolyte and mixed with the active electrode materials. The solid–electrolyte separator has a composition of Li$_{1+x+y}$Al$_x$Ti$_{2-x}$Si$_y$P$_{3-y}$O$_{12}$ (OHARA Inc, LICGC, AG01, conductivity: 10^{-4} Scm^{-1}, thickness: 150 μm). All the cells were assembled in an argon-filled glove box.

[25] **Material Characterization**

Morphology of the material was characterized with a field-emission scanning electron microscopy (FESEM, ZEISS, SUPRA 40). The particle size of LiFePO$_4$ was estimated using a laser scatterometer (Zetasizer Nano ZS, Malvern). Before the measurement, LiFePO$_4$ powder was dispersed in a viscous paraffin oil (refractive index: 1.475, dielectric constant: 2.2, viscosity: 1000 cP) to prevent
[30] fast sedimentation and stirred with a magnetic stirrer for 20 min.

2. Morphology and laser scattering particle size measurements of LiFePO$_4$
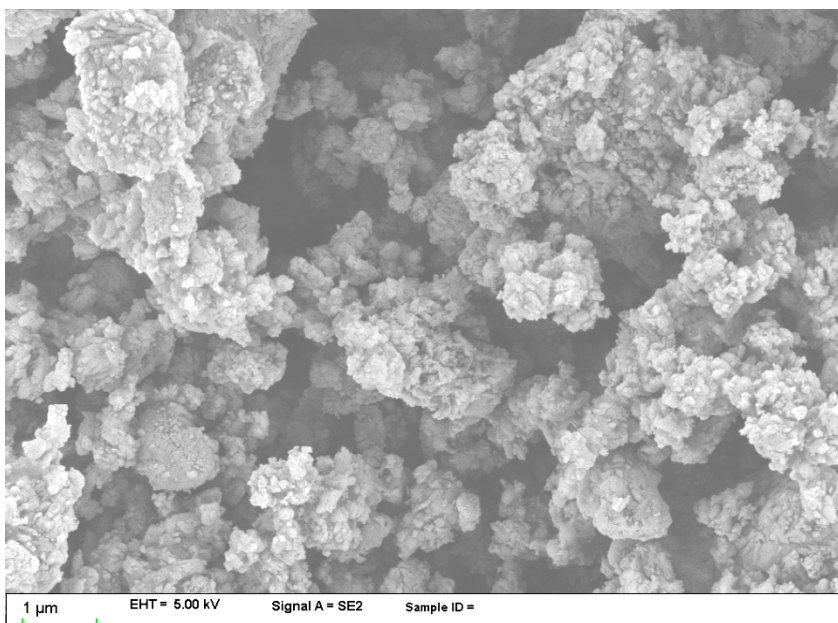
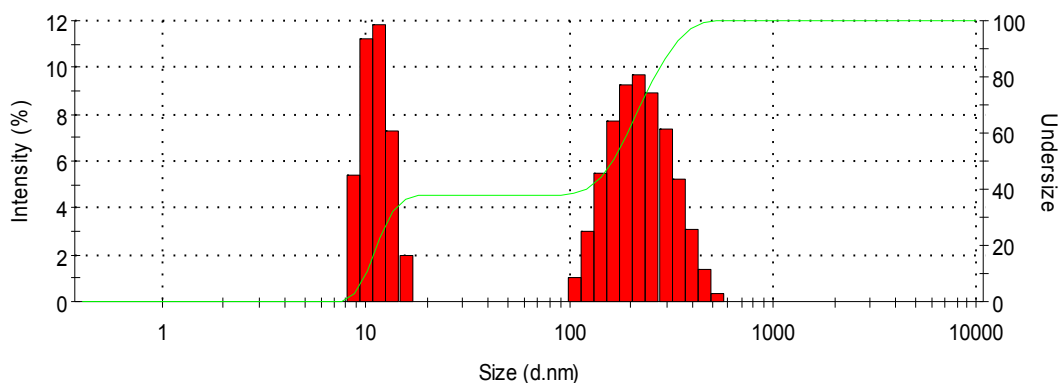**Figure S1.** SEM image of the as-received powder of LiFePO$_4$.

Figure S2. Particle size distribution of LiFePO$_4$ obtained from laser scattering measurement. The powder of LiFePO$_4$ was dispersed and stirred in paraffin oil to prevent fast sedimentation.

The LiFePO$_4$ powder used in this study is commercially available from Sigma-Aldrich with little carbon in the material. As the SEM images shown in Figure S1, the particles of LiFePO$_4$ have an irregular shape with size ranging from tens of nanometer to big agglomerations of up to a few microns. However, upon dispersing in paraffin oil, the agglomerations seem broken into small pieces as the particle size distribution revealed in Figure S2 by laser scattering measurement, where an apparent bimodal distribution was observed, with a significant portion of the particles centered at ~10 nm and the rest centered at ~200-300 nm.

3. Kinetics of chemical delithiation and lithiation.

The *in-situ* UV-Vis measurements of the redox shuttle molecules upon chemical delithiation and lithiation provide a means for investigating the kinetics of lithium insertion and extraction in LiFePO$_4$. As shown in Figure 3 in the main text, the optical densities (OD) of both redox shuttle

2

molecules change swiftly in the beginning the reaction, which then evolve gradually. The reactions complete after 50-60 min. The initial fast OD changes of $FcBr^{2+}$ and Fc are presumably a result of fast interfacial charge transfer between the redox molecules and materials, which are close to the surface. As the quantity of redox molecules is 5 times that of $LiFePO_4$/ $FePO_4$, the slow OD changes in the later stage is likely dominated by the transport of Li^+ within the particles. If we use the "effective" diffusion coefficient D_{Li+} to describe the kinetics of one dimensional Li^+ transport in the solid phase, then

$$D_{Li^+} = \frac{L^2}{2\tau}$$

Where L is the distance for Li^+ transport in the solid, which approximately is the radius of the particles. τ is the time constant for Li^+ transport, being ~50-60 min for both delithiation and lithiation in the largest particles (~200-500 nm). So D_{Li+} is calculated to be 10^{-14}-10^{-13} cm^2s^{-1}, in good agreement with the reported values.
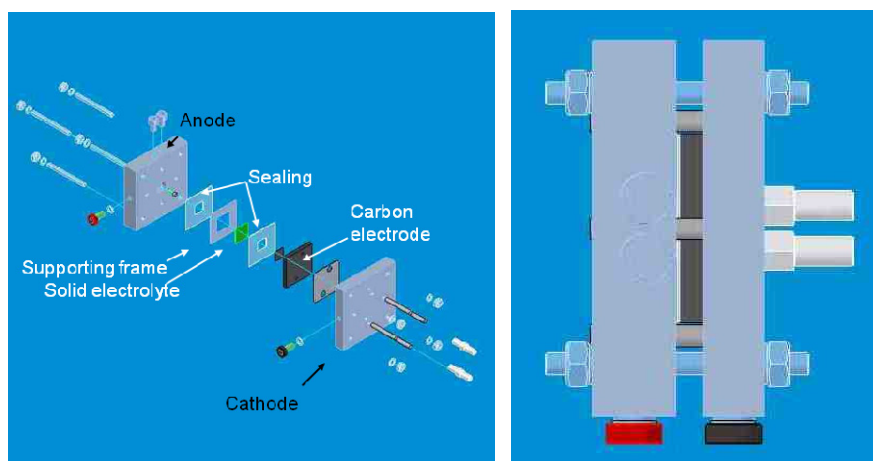
4. Configuration of RFLB half-cell.

Figure S3. Configuration of a RFLB half-cell. Left: exploded view; Right: top view.

5. Estimation of tank volumetric energy density of RFLB

In RFLB as energy is stored in solid phases, which is in contrast to the liquid phase in the conventional redox-flow batteries, the energy density of RFLB is expected to be much higher. With the combination of cathodic $LiFePO_4$ and anodic $Li_4Ti_5O_{12}$ as an example, the concentrations of Li^+ in the two materials are 22.8 and 21.9 M, considering their theoretical densities are 3.60 and 3.50 gcm^{-3}, respectively. If these two materials have a 50% porosity in the energy tanks, the volumetric energy density of RFLB would be 6-12 times as high as the state-of-the-art vanadium redox batteries (VRB), in which the concentration of vanadium species is normally 1-2 M. If in RFLB both cathodic Li^+-storage materials with higher potentials and anodic materials with lower potentials are used, much higher energy density could be achieved since the open circuit voltage of the aqueous solution-based VBR is only 1.40 V.